5202 *Inorg. Chem.* **2010**, *49*, 5202–5211
DOI: 10.1021/ic100322p

Inorganic Chemistry
Article

Synthesis, Characterization, and Theoretical Studies of Metal Complexes Derived from the Chiral Tripyridyldiamine Ligand Bn-CDPy3

Ahmed I. Abouelatta, Jason A. Sonk, Mirvat M. Hammoud, Danielle M. Zurcher, Joshua J. McKamie, H. Bernhard Schlegel, and Jeremy J. Kodanko*

Department of Chemistry, Wayne State University, 5101 Cass Avenue, Detroit, Michigan 48202

Received February 17, 2010

Synthesis and characterization of metal complexes of the chiral tripyridyldiamine ligand Bn-CDPy3 (**1**), derived from *trans*-1,2-diaminocyclohexane, are described, along with theoretical studies that support the experimental data. These studies confirm that a single coordination geometry, out of five possible, is favored for octahedral complexes of the type [M(Bn-CDPy3)Cl], where M equals Co(III), Fe(II), and Zn(II). A combination of X-ray crystallographic and NMR spectroscopic methods was used to define the structures of the complexes $[Co(Bn\text{-}CDPy3)Cl]Cl_2$ (**5**), $[Fe(Bn\text{-}CDPy3)Cl]X$ (X = $FeCl_4$, Cl, ClO_4, **6**−**8**), and $[Zn(Bn\text{-}CDPy3)Cl]_2ZnCl_4$ (**9**) in the solid state and in solution. Experimental and theoretical data indicate that the most stable coordination geometry for all complexes possesses the Cl group *trans* to a basic amine donor and three pyridyl donors adopting the *mer* geometry, with two pyridyl N-donors adopting a coplanar geometry with respect to the M−Cl bond and the third pyridyl donor perpendicular to that axis. Calculations indicate that the ability to favor a single geometry is born from the chiral ligand, which prefers to be in a single conformation in metal complexes due to steric interactions and electronic factors. Calculated structures of the complexes were used to locate key interactions among the various diastereomeric complexes that are proposed to create an energetic preference for the coordination geometry observed in the metal complexes of **1**.

Introduction

The transfer of chirality from an asymmetric ligand to a metal center has been a long-standing principle of coordination chemistry. Due to their ability to create an asymmetric environment around the metal center, chiral ligands have been used extensively in asymmetric synthesis and catalysis, as well as supramolecular chemistry. The ability to predict and control the coordination geometry of a ligand when bound to a metal center is certainly an important aspect of this chemistry, because the geometry can dictate the shape of the molecule and the asymmetric environment around the metal center.[1] Chirality can be introduced into a ligand by using building blocks that contain planar chiral or stereogenic centers. Of the various building blocks available, *trans*-1,2-diaminocyclohexane has been common, serving as the key chiral constituent in hundreds of asymmetric ligands. Thus, this important chiral diamine can be considered a privileged scaffold for ligand design.

The coordination chemistry of nitrogen-rich pentadentate ligands has received much attention (Figure 1). Pentadentate ligands display the unique ability to coordinate to an octahedral metal center with five donors, while leaving the sixth position open for binding to an additional group. This special binding mode has led the way to a variety of interesting reactivities not easily accessed by other ligand types. In particular, these ligands have demonstrated the ability to stabilize high-valent metal centers[2,3] and block bimolecular decay processes of reactive intermediates observed when using ligands of lower denticity. Also important has been their ability to participate in atom- or group-transfer reactions.[4] Groups found in the sixth position of such complexes have included oxo,[5−9]

*To whom correspondence should be addressed. E-mail: jkodanko@chem.wayne.edu.

(1) Knof, U.; Von Zelewsky, A. *Angew. Chem., Int. Ed.* **1999**, *38*, 303–322.
(2) Que, L. *Acc. Chem. Res.* **2007**, *40*, 493–500.
(3) Nam, W. *Acc. Chem. Res.* **2007**, *40*, 522–531.
(4) Bukowski, M. R.; Comba, P.; Lienke, A.; Limberg, C.; Lopez de Laorden, C.; Mas-Balleste, R.; Merz, M.; Que, L., Jr. *Angew. Chem., Int. Ed.* **2006**, *45*, 3446–3449.
(5) Klinker, E. J.; Kaizer, J.; Brennessel, W. W.; Woodrum, N. L.; Cramer, C. J.; Que, L., Jr. *Angew. Chem., Int. Ed.* **2005**, *44*, 3690–3694.
(6) Kaizer, J.; Klinker, E. J.; Oh, N. Y.; Rohde, J.-U.; Song, W. J.; Stubna, A.; Kim, J.; Münck, E.; Nam, W.; Que, L., Jr. *J. Am. Chem. Soc.* **2004**, *126*, 472–473.
(7) Bukowski, M. R.; Koehntop, K. D.; Stubna, A.; Bominaar, E. L.; Halfen, J. A.; Muenck, E.; Nam, W.; Que, L., Jr. *Science* **2005**, *310*, 1000–1002.
(8) Sastri, C. V.; Park, M. J.; Ohta, T.; Jackson, T. A.; Stubna, A.; Seo, M. S.; Lee, J.; Kim, J.; Kitagawa, T.; Muenck, E.; Que, L., Jr.; Nam, W. *J. Am. Chem. Soc.* **2005**, *127*, 12494–12495.
(9) Bautz, J.; Bukowski, M. R.; Kerscher, M.; Stubna, A.; Comba, P.; Lienke, A.; Munck, E.; Que, L., Jr. *Angew. Chem., Int. Ed.* **2006**, *45*, 5681–5684.
(10) Hazell, A.; McKenzie, C. J.; Nielsen, L. P.; Schindler, S.; Weitzer, M. *J. Chem. Soc., Dalton Trans.* **2002**, 310–317.
(11) Guajardo, R. J.; Tan, J. D.; Mascharak, P. K. *Inorg. Chem.* **1994**, *33*, 2838–2840.

 Published on Web 05/11/2010

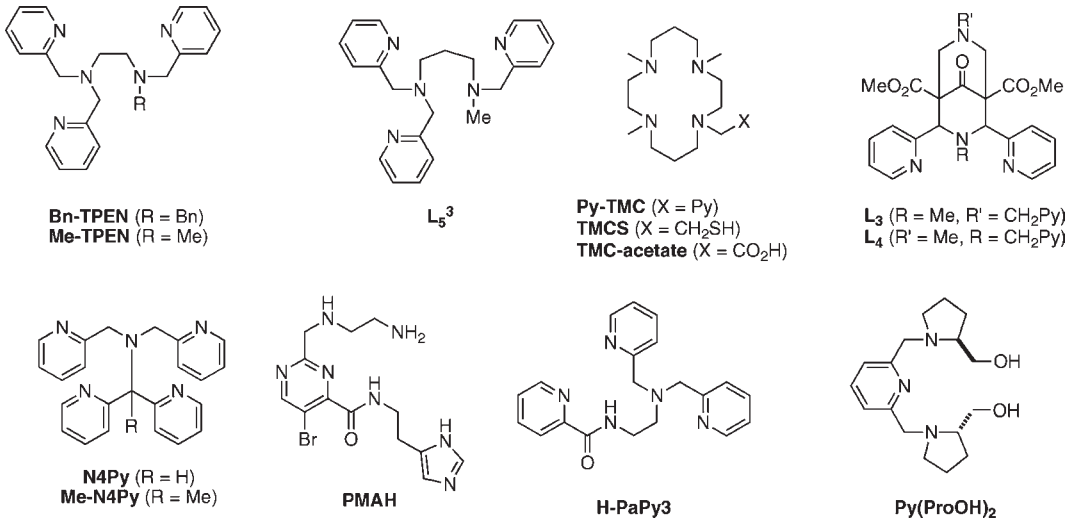

Figure 1. Examples of known pentadentate ligands containing multiple N-donors and their derivatives.

hydroperoxo,[10−12] azide,[13] imidio,[14] nitrosyl,[15] nitrido,[16] cyanide,[17] and halogens.[17] Despite such attention, the element of chirality has been noticeably absent in these ligands. In fact, there are only a few examples of chiral pentadentate ligands reported that contain similar nitrogen-rich donor sets.[18−24]

Considering there have been few reported examples of ligands of this type, we initiated studies to define new chiral pentadentate ligands with nitrogen-rich donor sets. To begin our studies, we chose to merge the privileged scaffold *trans*-1,2-diaminocyclohexane with the general structure of the R-TPEN class of pentadentate ligands (Figure 1). In this operation the ethyl bridge between the two basic amines of the parent Bn-TPEN was replaced with a cyclohexyl linker, yielding Bn-CDPy3 (Figure 2). While seemingly straightforward, the new cyclohexane motif added complexity and new questions surrounding the coordination chemistry of the chiral ligand. By differentiating the amines of the diaminocyclohexane backbone, the C_2 symmetry of the ligand is destroyed, creating a C_1 symmetric ligand in its place. This lowering of symmetry creates the opportunity for the ligand to access more coordination modes than possible for tetra- or hexadentate ligands derived from *trans*-1,2-diaminocyclohexane that carry identical donors on the two amine centers.[25−28] Furthermore, the element of chirality conferred by the cyclohexane linker would create the possibility for additional stereoisomeric coordination modes; that is, modes that were equivalent or enantiomeric in the case of the R-TPEN ligands would become diastereomeric in the case of the new chiral ligand. In this full paper, we expand on our initial studies that described the characterization of the complex [Co(Bn-CDPy3)Cl]Cl_2[29] and report that a single coordination geometry is preferred from five possible modes for transition metal complexes derived from the chiral pentadentate ligand Bn-CDPy3. In addition, we report theoretical studies that support these experimental observations, as well as molecular modeling studies that shed light on the origin of the remarkable control over coordination geometry that is observed with the asymmetric ligand Bn-CDPy3.

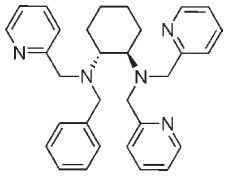

Figure 2. Structure of (*R*,*R*)-Bn-CDPy3 (**1**), a chiral pentadentate ligand.

Experimental Section

Instrumentation. All reagents were purchased from commercial suppliers and used as received. NMR spectra were recorded on a Varian FT-NMR Unity-300, Mercury-400, or Oxford-500 MHz spectrometer. Mass spectra were recorded on a Waters ZQ2000 single quadrupole mass spectrometer using an electrospray ionization source. IR spectra were recorded on a Nicolet

(12) Guajardo, R. J.; Hudson, S. E.; Brown, S. J.; Mascharak, P. K. *J. Am. Chem. Soc.* **1993**, *115*, 7971–7977.
(13) Berry, J. F.; Bill, E.; Bothe, E.; Weyhermueller, T.; Wieghardt, K. *J. Am. Chem. Soc.* **2005**, *127*, 11550–11551.
(14) Klinker, E. J.; Jackson, T. A.; Jensen, M. P.; Stubna, A.; Juhasz, G.; Bominaar, E. L.; Muenck, E.; Que, L., Jr. *Angew. Chem., Int. Ed.* **2006**, *45*, 7394–7397.
(15) Eroy-Reveles, A. A.; Leung, Y.; Beavers, C. M.; Olmstead, M. M.; Mascharak, P. K. *J. Am. Chem. Soc.* **2008**, *130*, 6650.
(16) Grapperhaus, C. A.; Mienert, B.; Bill, E.; Weyhermueller, T.; Wieghardt, K. *Inorg. Chem.* **2000**, *39*, 5306–5317.
(17) Ortega-Villar, N.; Ugalde-Saldivar, V. M.; Munoz, M. C.; Ortiz-Frade, L. A.; Alvarado-Rodriguez, J. G.; Real, J. A.; Moreno-Esparza, R. *Inorg. Chem.* **2007**, *46*, 7285–7293.
(18) Seitz, M.; Stempfhuber, S.; Zabel, M.; Schutz, M.; Reiser, O. *Angew. Chem., Int. Ed.* **2005**, *44*, 242–245.
(19) Gillard, R. D.; Newman, P. D.; Vagg, R. S.; Williams, P. A. *Inorg. Chim. Acta* **1995**, *233*, 79–84.
(20) Gosiewska, S.; Lutz, M.; Spek, A. L.; Klein Gebbink, R. J. M. *Inorg. Chim. Acta* **2007**, *360*, 405–417.
(21) Bernauer, K.; Pousaz, P. *Helv. Chim. Acta* **1984**, *67*, 796–803.
(22) Bernauer, K.; Pousaz, P.; Porret, J.; Jeanguenat, A. *Helv. Chim. Acta* **1988**, *71*, 1339–1348.
(23) Larionov, S. V.; Myachina, L. I.; Glinskaya, L. A.; Klevtsova, R. F.; Bizyaev, S. N.; Tkachev, A. V. *Russ. Chem. Bull.* **2007**, *56*, 1771–1774.
(24) Kurosaki, H.; Koike, H.; Omori, S.; Ogata, Y.; Yamaguchi, Y.; Goto, M. *Inorg. Chem. Commun.* **2004**, *7*, 1229–1232.
(25) Costas, M.; Tipton, A. K.; Chen, K.; Jo, D.-H.; Que, L., Jr. *J. Am. Chem. Soc.* **2001**, *123*, 6722–6723.
(26) Jensen, M. P.; Costas, M.; Ho, R. Y. N.; Kaizer, J.; Payeras, A. M.; Muenck, E.; Que, L., Jr.; Rohde, J.-U.; Stubna, A. *J. Am. Chem. Soc.* **2005**, *127*, 10512–10525.
(27) Sato, M.; Mori, Y.; Iida, T. *Synthesis* **1992**, 539–540.
(28) Mori, Y.; Sato, M.; Iida, T. *Chem. Lett.* **1992**, 469–472.
(29) Hammoud, M. M.; McKamie, J. J.; Heeg, M. J.; Kodanko, J. J. *Dalton Trans.* **2008**, 4843–4845.

FT-IR spectrophotometer. UV−vis spectra were recorded on a Varian Cary 50 spectrophotometer. CD spectral data were recorded on a Chirascan circular dichroism spectrophotometer. Reactions were performed under ambient atmosphere. Oxygen- and moisture-sensitive reactions were performed inside an MBraun Labmaster 130 glovebox. Molecular modeling studies were performed with the program MacPyMol.

Computational Details. All five isomers of the cobalt-, zinc-, and iron-containing structures were fully optimized using the TPSS pure functional[30] with an all-electron cc-pVTZ basis set[31−35] on the ligands and metals. Equilibrium geometries were confirmed using vibrational frequency analysis. For comparison, optimizations where also carried out with the B3LYP hybrid functional.[36−38] Single-point calculations were performed on the optimized structure of the ligand without the metal halide using the TPSS pure density functional with the cc-pVTZ basis set. NBO[39] analysis was used to look at the nature of the molecular orbitals of the calculated structures. NMR calculations were performed using the gauge-independent atomic orbital (GIAO) method[40−43] with the TPSS functional and the cc-pVTZ basis set. The reference in the NMR spectrum was TMS (tetramethylsilane) calculated using the same functional and basis set. Calculations of the UV−vis spectra utilized time-dependent density functional theory (TD-DFT)[44−50] with the long-range corrected LC-ωPBE functional[51−54] and the cc-pVTZ basis set. All calculations were performed using the development version of the Gaussian software suite.[55] Overlap studies with calculated structures were performed with MacPyMOL (see Supporting Information).

X-ray Crystallography. Diffraction data were measured on a Bruker X8 APEX-II kappa geometry diffractometer with Mo radiation and a graphite monochromator. Frames were collected at 100 K with the detector at 40 mm and 0.3 degrees between each frame and were recorded for 10 s. APEX-II[56] and SHELX[57] software were used in the collection and refinement of the models.

Crystals of [Co(Bn-CDPy3)Cl]Cl_2 (**5**) appeared as violet plates; 92 682 reflections were measured, yielding 17 503 unique data (R_{int} = 0.052). Hydrogen atoms in the complex were placed in calculated positions. The asymmetric unit contains two independent Co complexes and a solvent region consisting of four chloride ions, six water solvates, and one ethanol molecule. Of these, the ethanol and one water molecule were highly disordered, lying near the inversion center, and a reasonable chemical refinement was not possible. Spek's PLATON program was employed to account for approximately 66 e^- via SQUEEZE.[58] The highest ΔF peak (~2 e^-) was located in the vicinity of the disordered solvent.

Crystals of [Fe(Bn-CDPy3)Cl]ClO_4 (**8**) were yellow and irregular fragments. 69 185 points were integrated and merged into 13 686 independent data with R_{int} = 0.0343. Hydrogen atoms were placed in calculated positions. The asymmetric unit contains one Fe complex, one perchlorate counter ion, one equivalent of acetonitrile and one disordered equivalent of diethyl ether. The diethyl ether disorder was handled by assigning two sets of positions and holding these partial occupancy positions isotropic during refinement with their bond distances fixed. The highest difference map peaks (1−1.4 e^-) were in the vicinity of this disordered solvate.

(*R*,*R*)-*N*^{1}-Benzyl-*N*^{1},*N*^{2},*N*^{2}-tris(pyridin-2-ylmethyl)cyclohexane-1,2-diamine (Bn-CDPy3, 1). Enantioenriched **1** was synthesized according to the reported procedure starting from the enantioenriched starting material (1*R*,2*R*)-(−)-1,2-cyclohexanediamine (99% ee).[29] ^{1}H and ^{13}C NMR and mass spectral data for enantioenriched **1** matched data for the racemic compound. $[\alpha]_D$ = 51.1 (*c* 1.0, MeOH).

[Co(Bn-CDPy3)Cl]Cl_2 (5·5H_2O). The cobalt(III) complex [Co(Bn-CDPy3)Cl]Cl_2·5H_2O was prepared according to literature using the enantiopure (*R*,*R*)-Bn-CDPy3, **1**.[29] Mass, ^{1}H and ^{13}C NMR, and UV−vis spectral data matched with a racemic complex.

[Fe(Bn-CDPy3)Cl]Cl (7). A solution of ligand 1 (0.20 g, 0.418 mmol) in DCM (12 mL) was stirred with $FeCl_2$ (0.053 g, 0.418 mmol) inside the glovebox for 4 h, resulting in the formation of a yellow solution. The solution was filtered and concentrated inside the glovebox. The resultant golden yellow solid was recrystallized by vapor diffusion from MeCN/Et_2O inside the glovebox, yielding yellow needle crystals of **7**·3H_2O (0.16 g, 63%). Mp = 155−156 °C; χ_{mol} = 4.90 μ_B. ^{1}H NMR (CD_3OD): δ 160.2, 140.5, 108.4, 99.1, 96.4, 89.1, 57.4, 56.6, 52.4, 49.5, 41.6, 40.0, 26.1, 24.4, 19.2, 15.4, 11.5, 9.4, 7.5, 4.5, 3.0, 2.5, 1.9, 1.7, 1.3, −0.8, −7.4, −21.3, −24.5. IR (thin film): 3411(s), 3060(w), 3027(w), 2933(s), 2860(m), 2359(w), 1602(s), 1570(m), 1482(s), 1443(s), 1384(w), 1352(w), 1316(w), 1296(w), 1245(w), 1204(m), 1155(m), 1099(m), 1077(m), 1052(m), 1016(m), 978(w), 960(w),

(30) Tao, J.; Perdew, J. P.; Staroverov, V. N.; Scuseria, G. E. *Phys. Rev. Lett*. **2003**, *91*, 146401.
(31) Woon, D. E.; Dunning, T. H. J. *J. Chem. Phys*. **1993**, *98*, 1358–1371.
(32) Kendall, R. A.; Dunning, T. H. J.; Harrison, R. J. *J. Chem. Phys*. **1992**, *96*, 6796–6806.
(33) Dunning, T. H. J. *J. Chem. Phys*. **1989**, *90*, 1007–1023.
(34) Peterson, K. A.; Woon, D. E.; Dunning, T. H. J. *J. Chem. Phys*. **1994**, *100*, 7410–7415.
(35) Wilson, A. K.; van Mourik, T.; Dunning, T. H. *J. Mol. Struct*. **1996**, *388*, 339–349.
(36) Becke, A. D. *J. Chem. Phys*. **1993**, *98*, 5648–5652.
(37) Lee, C.; Yang, W.; Parr, R. G. *Phys. Rev. B* **1988**, *37*, 785.
(38) Miehlich, B.; Savin, A.; Stoll, H.; Preuss, H. *Chem. Phys. Lett*. **1989**, *157*, 200–206.
(39) Glendening, E. D.; Reed, A. E.; Carpenter, J. E.; Weinhold, F. *QCPE Bull*. **1990**, *10*, 58.
(40) McWeeny, R. *Phys. Rev*. **1962**, *126*, 1028.
(41) Wilson, S. M.; Wiberg, K. B.; Cheeseman, J. R.; Frisch, M. J.; Vaccaro, P. H. *J. Phys. Chem. A* **2005**, *109*, 11752–11764.
(42) Cheeseman, J. R.; Trucks, G. W.; Keith, T. A.; Frisch, M. J. *J. Chem. Phys*. **1996**, *104*, 5497–5509.
(43) Ditchfield, R. *Mol. Phys*. **1974**, *27*, 789–807.
(44) Bauernschmitt, R.; Ahlrichs, R. *Chem. Phys. Lett*. **1996**, *256*, 454–464.
(45) Casida, M. E.; Jamorski, C.; Casida, K. C.; Salahub, D. R. *J. Chem. Phys*. **1998**, *108*, 4439–4449.
(46) Stratmann, R. E.; Scuseria, G. E.; Frisch, M. J. *J. Chem. Phys*. **1998**, *109*, 8218–8224.
(47) Van Caillie, C.; Amos, R. D. *Chem. Phys. Lett*. **1999**, *308*, 249–255.
(48) Van Caillie, C.; Amos, R. D. *Chem. Phys. Lett*. **2000**, *317*, 159–164.
(49) Furche, F.; Ahlrichs, R. *J. Chem. Phys*. **2002**, *117*, 7433–7447.
(50) Scalmani, G.; Frisch, M. J.; Mennucci, B.; Tomasi, J.; Cammi, R.; Barone, V. *J. Chem. Phys*. **2006**, *124*, 094107–094115.
(51) Tawada, Y.; Tsuneda, T.; Yanagisawa, S.; Yanai, T.; Hirao, K. *J. Chem. Phys*. **2004**, *120*, 8425–8433.
(52) Vydrov, O. A.; Scuseria, G. E. *J. Chem. Phys*. **2006**, *125*, 234109–.
(53) Vydrov, O. A.; Scuseria, G. E.; Perdew, J. P. *J. Chem. Phys*. **2007**, *126*, 154109–.
(54) Vydrov, O. A.; Heyd, J.; Krukau, A. V.; Scuseria, G. E. *J. Chem. Phys*. **2006**, *125*, 074106–074109.
(55) Frisch, M. J.; Trucks, G. W.; Schlegel, H. B.; Scuseria, G. E.; Robb, M. A.; Cheeseman, J. R.; Scalmani, G.; Barone, V.; Mennucci, B.; Petersson, G. A.; Nakatsuji, H.; Caricato, M.; Li, X.; Hratchian, H. P.; Izmaylov, A. F.; Bloino, J.; Zheng, G.; Sonnenberg, J. L.; Hada, M.; Ehara, M.; Toyota, K.; Fukuda, R.; Hasegawa, J.; Ishida, M.; Nakajima, T.; Honda, Y.; Kitao, O.; Nakai, H.; Vreven, T.; Montgomery, J. A., Jr.; Peralta, J. E.; Ogliaro, F.; Bearpark, M.; Heyd, J. J.; Brothers, E.; Kudin, K. N.; Staroverov, V.; Kobayashi, R.; Normand, J.; Raghavachari, K.; Rendell, A.; Burant, J. C.; Iyengar, S. S.; Tomasi, J.; Cossi, M.; Rega, N.; Millam, J. M.; Klene, M.; Knox, J. E.; Cross, J. B.; Bakken, V.; Adamo, C.; Jaramillo, J.; Gomperts, R.; Stratmann, R. E.; Yazyev, O.; Austin, A. J.; Cammi, R.; Pomelli, C.; Ochterski, J. W.; Martin, R. L.; Morokuma, K.; Zakrzewski, V. G.; Voth, G. A.; Salvador, P.; Dannenberg, J. J.; Dapprich, S.; Parandekar, P. V.; Mayhall, N. J.; Daniels, A. D.; Farkas, O.; Foresman, J. B.; Ortiz, J. V.; Cioslowski, J.; Fox, D. J. *Gaussian*, Revision H.01 ed.; Gaussian, Inc.: Wallingford, CT, 2009.
(56) *APEX II collection and processing programs*; Bruker AXS Inc.: Madison WI, **2009**.
(57) Sheldrick, G. M. *Acta Crystallogr*. **2008**, *A64*, 112–122.
(58) Spek, A. L. *J. Appl. Crystallogr*. **2003**, *36*, 7–13.

931(w), 884(w), 816(w), 758(s), 708(s) cm^{-1}. Anal. Calcd for $C_{31}H_{41}Cl_2FeN_5O_3$ (**3**·$3H_2O$): C, 56.55; H, 6.28; N, 10.64. Found: C, 56.44; H, 5.89; N, 10.67.

[Fe(Bn-CDPy3)Cl]ClO_4 (8). The complex [Fe(Bn-CDPy3)Cl]ClO_4 (**4**) was obtained by ion exchange of [Fe(Bn-CDPy3)Cl]Cl (**7**) and $AgClO_4$. A stock solution of $AgClO_4$ (0.0365 g, 0.175 mmol) in MeCN (2.5 mL) was prepared in the glovebox. The complex [Fe(Bn-CDPy3)Cl]Cl (**7**) (0.02 g, 0.035 mmol) was dissolved in MeCN (0.5 mL), mixed with 0.5 mL of the prepared $AgClO_4$ solution, and stirred for 5 min, resulting in formation of a white precipitate (AgCl). The precipitate was removed by filtration, and [Fe(Bn-CDPy3)Cl]ClO_4 was crystallized by vapor diffusion with 3 mL of Et_2O, yielding yellow crystals of **8**·H_2O (10 mg, 34%). These crystals were subjected to X-ray crystallographic analysis. Mp = 146−148 °C. IR (thin film): 3409(s), 3065(w), 2936(m), 2860(w), 1657(m), 1604(m), 1482(w), 1444(m), 1142(s), 1109(s), 1090(s), 1017(w), 763(m), 708(w), 661(w), 625(m) cm^{-1}. Anal. Calcd for $C_{31}H_{37}Cl_2FeN_5O_5$ (**4**·H_2O): C, 54.24; H, 5.43; N; 10.20. Found: C, 54.20; H, 5.35; N, 10.34.

[Zn(Bn-CDPy3)Cl]$_2$$ZnCl_4$ (9). The ligand (*R*,*R*)-Bn-CDPy3 (0.20 g, 0.418 mmol) was dissolved in THF (5 mL) and stirred with $ZnCl_2$ (0.085 g, 0.627 mmol) inside the glovebox overnight. A white precipitate formed immediately and then disappeared upon stirring. The solution was concentrated inside the glovebox. The resultant lightly colored solid was stirred with ether overnight in the glovebox. The suspension was filtered, and the colorless solid was dried *in vacuo* then outside the glovebox in a Shlenk tube at 120 °C overnight to remove traces of THF, yielding a colorless solid (0.27 g, 47%). Mp = 190 °C (dec). ^{1}H NMR (CD_3OD): δ 9.24 (d, J = 4.9 Hz, 1H), 8.84 (d, J = 4.9 Hz, 1H), 8.02 (m, 1H), 7.93 (m, 1H), 7.80 (m, 1H), 7.72 (d, J = 4.9 Hz, 1H), 7.59 (d, J = 8.1 Hz, 1H), 7.49 (m, 3H), 7.37 (m, 7 H), 4.82 (d, J = 17.8 Hz, 1H), 4.70 (d, J = 15.4 Hz, 1H), 4.58 (d, J = 13.8 Hz, 1H), 4.37 (d, J = 16.2 Hz, 1H), 4.20 (d, J = 15.4 Hz, 1H), 3.94 (d, J = 17.0 Hz, 2H), 3.47 (d, J = 13.8 Hz, 1H), 3.28 (m, 1H), 2.04 (d, J = 13.0 Hz, 1H), 1.91 (dt, J = 11.4, 3.2 Hz, 1H), 1.69 (d, J = 17 Hz, 1H), 1.60 (dt, J = 12.2, 3.2 Hz, 1H), 1.45 (d, J = 12.2 Hz, 1H), 1.19 (m, 2H), 0.98 (m, 1H), 0.87 (m, 1H). ^{13}C NMR (CD_3OD): δ 155.8, 155.7, 154.5, 148.1, 147.8, 145.9, 140.6, 140.4, 139.7, 134.6, 130.7, 128.6, 125.3, 124.6, 124.5, 123.9, 123.6, 123.5, 68.8, 64.0, 62.8, 62.5, 54.5, 53.7, 29.2, 26.1, 24.6, 24.5. IR (thin film): 3466(s), 3061(w), 2938(m), 2861(w), 2281(w), 1604(s), 1574(m), 1484(m), 1443(s), 1384(w), 1315(w), 1295(w), 1204(w), 1156(w), 1101(w), 1084(w), 1053(m), 1019(m), 978(w), 934(w), 885(w), 853(w), 763(s), 708(m) cm^{-1}. Anal. Calcd for $C_{62}H_{72}Cl_6N_{10}OZn_3C$ (**5**·H_2O): C, 53.87; H, 5.25; N, 10.13. Found: C, 53.81; H, 5.08; N, 9.91.[59] LRMS (ESMS): 576.2 (ZnBn-CDPy3Cl).

Results

Synthesis. Synthesis of the ligand Bn-CDPy3 began from the dipyridyldiamine **2**, which is available in two steps from the commercially available starting material *trans*-1,2-diaminocyclohexane.[29] Treatment of **2** with one equivalent of 2-pyridinecarboxaldehyde in the presence of 4 Å molecular sieves gave aminal **3**, a stable compound that was isolable by alumina chromatography, in 88% yield. Reduction of the aminal using $NaBH_3CN$ and TFA gave the tripyridyldiamine **4** in 96% yield, which was alkylated with BnBr to give Bn-CDPy3 in 99% yield and 84% overall yield from **2**. The late stage introduction of the benzyl group during the synthesis of **1** was ideal, because analogues of **1** with different R-groups can be prepared readily from **4**. For the studies presented herein, it was necessary to prepare the ligand in racemic form,

Scheme 1. Synthesis of Bn-CDPy3 (**1**)

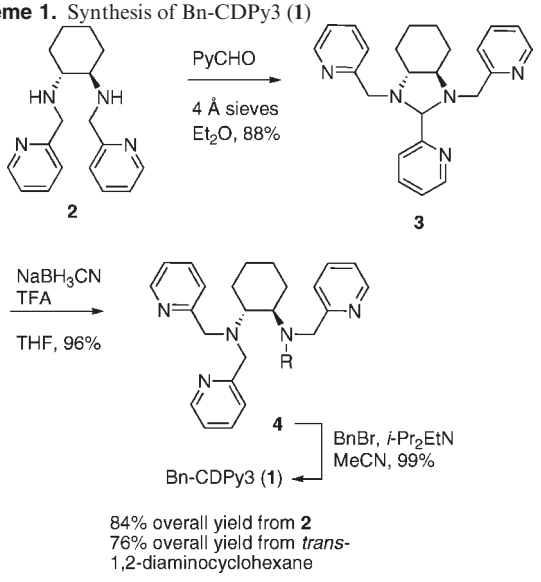

Scheme 2. Synthesis of Bn-CDPy3 Metal Complexes[a]

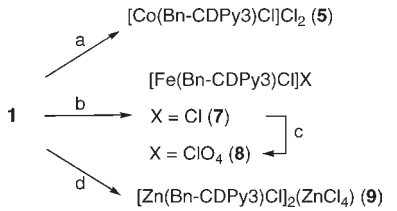

[a] (a) *trans*-[$Co(Py)_4Cl_2$]Cl·$6H_2O$, CH_2Cl_2, 12 h, dark, 79%. (b) $FeCl_2$, DCM, 4 h, 63%. (c) $AgClO_4$, MeCN, 34%. (d) $ZnCl_2$, THF, 47%.

starting from racemic *trans*-1,2-diaminocyclohexane, and in enantioenriched form, starting from the enantioenriched ligand (1*R*,2*R*)-(−)-1,2-cyclohexanediamine (99% ee). X-ray crystallographic studies were carried out with racemic ligand **1** in order to facilitate the crystallization process (metal complexes crystallized as racemates in the achiral space group $P\bar{1}$, *vide infra*), and complexes derived from the enantioenriched **1** were used for CD studies.

Cobalt, zinc, and iron metal complexes derived from **1** were synthesized (Scheme 2). The Co(III) complex was prepared by treating the ligand **1** with 1 equiv of *trans*-[$Co(Py)_4Cl_2$]Cl·$6H_2O$ in CH_2Cl_2 in the dark. After 12 h a purple solid was isolated that contained the complex [Co(Bn-CDPy3)Cl]Cl_2 (**5**) as a mixture of stereoisomers, with the one isomer major, one minor (5:1 major:minor) and trace amounts of other isomers. Recrystallization of the purple solid using EtOH with Et_2O vapor diffusion enriched the sample and gave purple plates of **5** as a >10:1 mixture of major to minor isomers, as evidenced by ^{1}H NMR analysis. The reaction of **1** in CH_2Cl_2 with 1 equiv of $FeCl_3$·$6H_2O$ in EtOH produced a complex mixture of products. Trace amounts of the complex [Fe(Bn-CDPy3)Cl]($FeCl_4$) (**6**) were obtained from this reaction and were identified by X-ray crystallographic analysis (see Supporting Information for structure). Attempts to obtain preparative amounts of **6** and a satisfactory elemental analysis of the material were unsuccessful. Therefore, an alternative synthesis of an Fe(II) complex was devised. Reaction of **1** with 1 equiv of $FeCl_2$ in CH_2Cl_2, followed by recrystallization from MeCN with Et_2O vapor diffusion,

(59) Jackson, W. G.; Sargeson, A. M.; Tucker, P. A.; Watson, A. D. *J. Am. Chem. Soc.* **1981**, *103*, 533–540.

Table 1. X-ray Crystallographic Data for **5** and **8**

parameter	[Co(Bn-CDPy3)Cl]Cl_2 (**5**)	[Fe(Bn-CDPy3)Cl]ClO_4 (**8**)
empirical formula	$C_{32}H_{44}Cl_3Co_1N_5O_{3.5}$	$C_{37}H_{48}Cl_2FeN_6O_5$
fw	720.00	783.56
cryst syst	triclinic	triclinic
space group	$P\bar{1}$	$P\bar{1}$
a (Å)	14.5658(3)	9.4228(3)
b (Å)	14.8438(3)	15.1824(5)
c (Å)	18.4793(4)	15.2967(8)
α (deg)	107.3480(1)	114.517(2)
β (deg)	105.8420(1)	97.436(2)
γ (deg)	96.4300(1)	102.973(2)
V (Å^3)	3586.6(1)	1878.1(1)
Z	4	2
final R indices [$I > 2\sigma(I)$]	R1 = 0.0457, wR2 = 0.1222	R1 = 0.0509, wR2 = 0.1421
R indices (all data)	R1 = 0.0642, wR2 = 0.1296	R1 = 0.0614, wR2 = 0.1489

gave the iron complex [Fe(Bn-CDPy3)Cl](Cl) (**7**) as a microcrystalline yellow solid in 63% yield. Because this material was not suitable for X-ray crystallographic analysis, the iron complex [Fe(Bn-CDPy3)Cl](ClO_4) (**8**) was prepared by ion exchange of **7** with 1 equiv of $AgClO_4$ in MeCN. Crystals of **8** suitable for X-ray analysis were grown from MeCN with Et_2O vapor diffusion. Reaction of the ligand **1** with 1.5 equiv of $ZnCl_2$ in THF produced the complex [Zn(Bn-CDPy3)Cl]$_2ZnCl_4$ (**9**), which was obtained as a colorless solid in 47% yield after washing with Et_2O.

X-ray Crystallographic Studies. X-ray crystallographic data for compounds **5** and **8** (see Supporting Information for **6**) and the parameters of data collections are described in Table 1. Tables 2 and 3 list selected bond lengths and bond angles, respectively.

The Co(III) complex **5** crystallizes as a racemate in the triclinic space group $P\bar{1}$, with $Z = 4$. Two enantiomeric dications of $[Co(Bn\text{-}CDPy3)Cl]^{2+}$ that are nearly identical in structure are located in the asymmetric unit in addition to four chloride anions, consistent with the complex bearing a Co(III) center. Due to their similarity, structural parameters for only one of the dications are described herein; parameters for the second dication can be found in the Supporting Information. The cobalt center has a mixed N and Cl (N_5Cl) donor atom set in which *mer* geometry is adopted by the three pyridine donors (Figure 3). The coordination environment around the metal center possesses a slightly distorted octahedral geometry, with bond angles ranging from 84.09(8)° to 97.19(7)°. The basic amine N-donor N(1) has a significantly shorter bond length to Co(1), measuring 1.961(2) Å, than the Co(1)−N(2) distance of 2.016(2) Å. Bond lengths Co(1)−N(3), Co(1)−N(4), and Co(1)−N(5) are nearly identical, at 1.939(3), 1.954(3), and 1.946(3) Å, respectively. The Co(1)−Cl(1) bond length is 2.241(1) Å. All the bond lengths are consistent with the dication of $[Co(Bn\text{-}CDPy3)Cl]^{2+}$ containing a low-spin Co(III) metal center.[29]

Crystallographic data for complexes **6** and **8** revealed that the $[Fe(Bn\text{-}CDPy3)Cl]^{+}$ cation adopts a solid-state conformation that is nearly identical between the two compounds, with little influence from the tetrachloroferrate or perchlorate counteranion (see Figure 4 for **8** and Supporting Information for **6**). The Fe^{II} complex **8** crystallizes as a racemate in the triclinic space group $P\bar{1}$, with $Z = 2$. The iron center contains a N_5Cl donor atom set in which *mer* geometry is adopted by the three pyridyl donors. The coordination environment of the ferrous center shows a slightly distorted octahedral geometry with bond angles ranging from 78.32(5)° to 104.09(4)°. For **8**, the Fe(1)−N(1) bond length at 2.236(1) Å is significantly shorter than the Fe(1)−N(2) bond length of 2.268(1) Å. Bond lengths between the pyridyl donors and the iron centers, Fe(1)−N(3), Fe(1)−N(4), and Fe(1)−N(5), are 2.163(1), 2.202(1), and 2.182(1) Å, respectively. Bond lengths to the iron center in **8** are in good agreement with $[Fe-N5]_{average}$ distances of the paramagnetic $[Fe^{II}(Bn\text{-}Tpen)X]$ complexes, indicating that the complexes contain a high-spin ($S = 2$) Fe(II) ion.[60] The Fe(1)−Cl(1) bond length for **8** is 2.3390(4) Å.

Table 2. Selected Bond Lengths (Å) for **5** and **8**

bond	[Co(Bn-CDPy3)Cl]Cl_2 (**5**)	bond	[Fe(Bn-CDPy3)Cl]ClO_4 (**8**)
Co(1)−N(1)	1.961(2)	Fe(1)−N(1)	2.236(1)
Co(1)−N(2)	2.016(2)	Fe(1)−N(2)	2.268(1)
Co(1)−N(3)	1.939(3)	Fe(1)−N(3)	2.163(1)
Co(1)−N(4)	1.954(3)	Fe(1)−N(4)	2.202(1)
Co(1)−N(5)	1.946(3)	Fe(1)−N(5)	2.182(1)
Co(1)−Cl(1)	2.241(1)	Fe(1)−Cl(1)	2.3390(4)

Spectroscopic Studies

NMR Spectroscopy. ^{1}H NMR spectroscopic data for compounds **5**, **7**, and **9** revealed a distinct pattern for the pyridyl C−H resonances, consistent with the compounds adopting the same conformation in solution. Resonances observed in the ^{1}H NMR spectrum of the Co(III) complex **5** in CD_3OD lie between 9.70 and 1.08 ppm, confirming the compound is a low-spin diamagnetic complex. An expansion of the aromatic region of the ^{1}H NMR spectrum of **5** is shown in Figure 5a. In this spectrum, two resonances corresponding to the protons found on the 2-position of the pyridine rings are shifted downfield to 9.70 and 9.04 ppm, while the third 2-pyridyl C−H resonance is shifted upfield to 7.34 ppm (see red arrows). This assignment agrees well with calculated data and also with literature precedence (*vide infra*).[5] A similar pattern was observed in the ^{1}H NMR spectrum of the diamagnetic Zn(II) complex **9** (Figure 5b), with resonances located at 9.24, 8.84, and 7.72 ppm, consistent with **9** adopting a similar conformation to **5**. The complex [Fe(Bn-CDPy3)Cl]Cl (**7**) showed a paramagnetically shifted and relatively sharp ^{1}H NMR spectrum, with resonances ranging from −25 to 160 ppm (Figure 5c). The high-spin nature of **7** was confirmed in the solid state with molar susceptibility of 4.90 μ_B, which agrees well for a $S = 2$ Fe(II) compound. Resonances in the ^{1}H NMR spectrum of **7** that were broad and located the furthest downfield were assigned to the 2-pyridyl C−H protons based on precedence.[61] Interestingly, the same pattern is evident in the paramagnetic ^{1}H NMR spectrum of **7** as was observed for the diamagnetic compounds **5** and **7**. Namely, two protons are

(60) Bernal, I.; Jensen, I. M.; Jensen, K. B.; McKenzie, C. J.; Toftlund, H.; Tuchagues, J.-P. *J. Chem. Soc., Dalton Trans.* **1995**, 3667–3675.
(61) Britovsek, G. J. P.; England, J.; White, A. J. P. *Inorg. Chem.* **2005**, *44*, 8125–8134.

Table 3. Selected Bond Angles (deg) for **5** and **8**

bond angle	[Co(Bn-CDPy3)Cl]Cl_2 (**5**)	bond angle	[Fe(Bn-CDPy3)Cl]ClO_4 (**8**)
N(1)−Co(1)−Cl(1)	178.83(6)	N(1)−Fe(1)−Cl(1)	172.08(4)
N(2)−Co(1)−Cl(1)	94.34(5)	N(2)−Fe(1)−Cl(1)	100.32(4)
N(3)−Co(1)−Cl(1)	94.74(6)	N(3)−Fe(1)−Cl(1)	104.09(4)
N(4)−Co(1)−Cl(1)	94.18(6)	N(4)−Fe(1)−Cl(1)	94.43(4)
N(5)−Co(1)−Cl(1)	85.39(6)	N(5)−Fe(1)−Cl(1)	95.28(4)
N(1)−Co(1)−N(2)	86.80(7)	N(1)−Fe(1)−N(2)	78.39(5)
N(3)−Co(1)−N(1)	84.11(8)	N(4)−Fe(1)−N(1)	78.32(5)
N(3)−Co(1)−N(2)	170.58(8)	N(4)−Fe(1)−N(2)	102.43(5)
N(3)−Co(1)−N(4)	84.63(8)	N(3)−Fe(1)−N(1)	78.32(5)
N(3)−Co(1)−N(5)	94.16(8)	N(3)−Fe(1)−N(4)	82.34(5)
N(4)−Co(1)−N(1)	85.90(8)	N(3)−Fe(1)−N(2)	154.70(5)
N(4)−Co(1)−N(2)	97.19(7)	N(3)−Fe(1)−N(5)	94.69(5)
N(5)−Co(1)−N(1)	94.50(8)	N(5)−Fe(1)−N(1)	92.01(5)
N(5)−Co(1)−N(2)	84.09(8)	N(5)−Fe(1)−N(4)	170.26(5)
N(5)−Co(1)−N(4)	178.68(8)	N(5)−Fe(1)−N(2)	76.39(5)

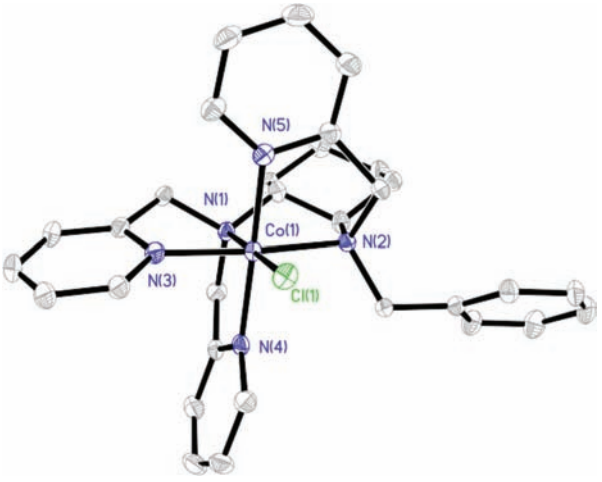

Figure 3. ORTEP diagram of the dication $[Co(Bn\text{-}CDPy3)Cl]^{2+}$ from compound **5**. Thermal ellipsoids are shown at 50% probability. Hydrogen atoms are omitted for clarity.

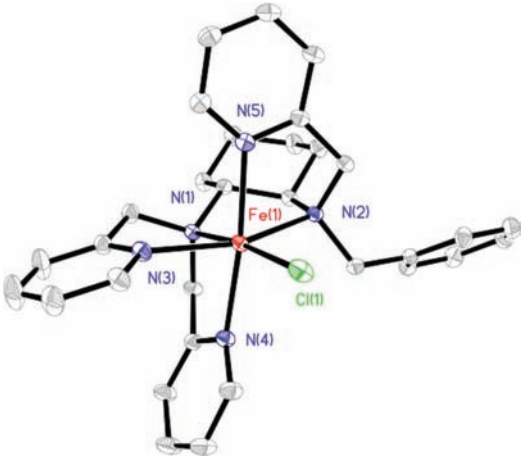

Figure 4. ORTEP diagram of the cation $[Fe(Bn\text{-}CDPy3)Cl]^{+}$ from **8**. Thermal ellipsoids are shown at 50% probability. Hydrogen atoms are omitted for clarity.

located downfield at 160 and 141 ppm, while the third is upfield at 89 ppm.

Because X-ray crystallographic data for the Zn(II) complex **9** were not available, additional NMR data were acquired in order to support the structural assignment of **9**. A combination of COSY, DEPT, and HMQC experiments were used to define protons and carbons in isolated spin systems in **9**, and NOESY data were used to identify close contacts between protons through space. Key protons used in the structural assignment are indicated in Figure 6; a full assignment of all protons is located in the Supporting Information. Analysis of HMQC data indicated that the two methine protons of the cyclohexyl ring, H(6) and H(1), were located at 1.91 and 3.28 ppm, respectively, in the ^{1}H NMR spectrum of **9**. The methylene proton H(13B) showed strong cross-peaks with H(6) and H(2B) in the NOESY spectrum, consistent with this proton lying between the two axial protons, a key structural feature of the preferred coordination geometry (*vide infra*). The pyridyl proton H(21) was assigned according to COSY data, which indicated that the proton H(24), assigned as the resonance furthest upfield in the ^{1}H NMR spectrum at 7.72 ppm, was in the same ring as H(21). This proton showed a strong cross-peak in the NOESY spectrum with H(19A), which was connected to H(5A), to H(1), and finally to H(7A).

UV−Vis Spectroscopy. The Fe(II) complex **7** dissolved in MeOH to form a yellow solution. The UV−vis absorption spectra of complex **7** showed two absorbances with λ_{max} at 413 and 362 nm, with ε = 1910 and 1790 M^{-1} cm^{-1}, respectively (Figure 7). The intensities of these bands are in good agreement with data for similar high-spin Fe(II) complexes, which agrees well with the paramagnetic shifts observed in ^{1}H NMR spectrum obtained for **7** in CD_3OD, as well as the solid-state magnetic susceptibility data.[62] The Co(III) complex **5** gives a purple solution with an absorption maximum at λ_{max} = 555 nm, ε = 159 M^{-1} cm^{-1} with a shoulder at 388 nm (Figure 7).

CD Spectroscopy. CD spectroscopic analysis of the chiral pentadentate ligand (*R*,*R*)-Bn-CDPy3 (**1**) and the Zn(II) complex **9** revealed no CD activity in the range 200−800 nm. On the other hand, both the Co(III) complex **5** and the Fe(II) complex **7** showed Cotton effects (Figure 8). In the case of the enantioenriched Co(III) complex **5**, two major features were observed in the CD spectrum. A positive maximum is located at 415 nm, along with a bisignate couplet centered at the maximum absorbance of **5** (550 nm), characteristic of exciton splitting. In contrast, complex **7** showed a negative maximum at 508 nm, with no exciton coupling.

(62) Ortega-Villar, N.; Ugalde-Saldivar, V. M.; Munoz, M. C.; Ortiz-Frade, L. A.; Alvarado-Rodriguez, J. G.; Real, J. A.; Moreno-Esparza, R. *Inorg. Chem.* **2007**, *46*, 7285–7293.

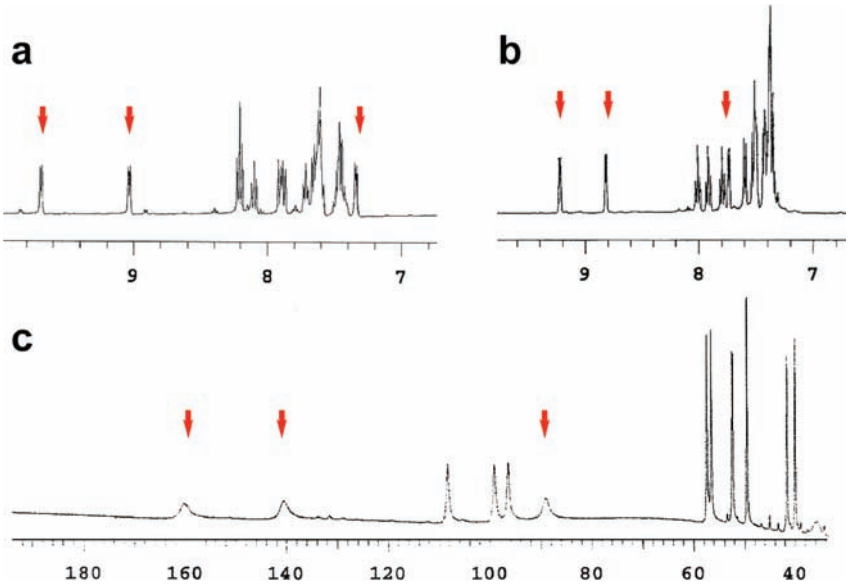

Figure 5. Expansions of ^{1}H NMR spectra of [Co(Bn-CDPy3)Cl]Cl_2 (**5**, spectrum a), [Zn(Bn-CDPy3)Cl]$_2ZnCl_4$ (**9**, spectrum b), and [Fe(Bn-CDPy3)Cl]Cl (**7**, spectrum c) in CD_3OD. A distinct pattern of two downfield and one upfield resonance (labeled with red arrows) was observed for the 2-pyridyl C−H protons of compounds **5**, **7**, and **9**. A minor amount of an unknown stereoisomer is present in the sample of **5**. Full spectra can be found in the Supporting Information.

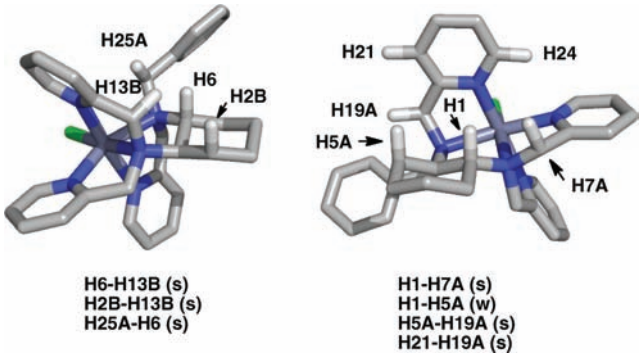

Figure 6. Three-dimensional models of [Zn(Bn-CDPy3)Cl]$^+$ with most hydrogen atoms omitted for clarity. Select hydrogen atoms showing NOE contacts are labeled with intensities of strong (s) or weak (w). Models are based on the calculated structure for [Zn(Bn-CDPy3)Cl]$^+$ (*vide infra*). See Supporting Information for further details.

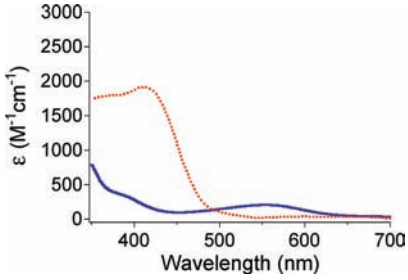

Figure 7. UV−vis spectra of **5** (blue line) and **7** (red, dotted line) in MeOH.

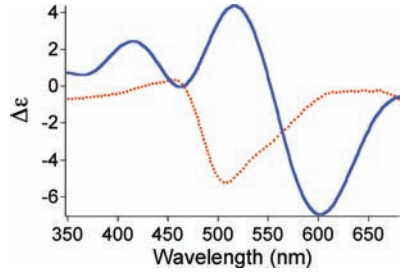

Figure 8. CD spectra of **5** (blue line) and **7** (red, dotted line) in MeOH.

Calculated Structures and Energetics

As shown in Figure 9, five isomers can be constructed for M(Bn-CDPy3)Cl. The calculated relative energies are summarized in Table 4 for M = Co(III), Fe(II), and Zn(II). Results for the B3LYP calculations are available in the Supporting Information. For all of the complexes considered, the calculations predict isomer C to be the lowest energy, in good agreement with the X-ray crystallographic data for Co(III) and Fe(II) complexes and the NMR data for the Zn(II) complex. The metal−ligand bond lengths and angles are collected in the Supporting Information and compare very well with the available experimental structural data. For isomer C the rmsd for the heavy atoms in the crystal structure versus calculated structure is 0.182 Å for the Co(III) complex and 0.139 Å for the Fe(II) complex. The bond lengths for the d^6 Co(III) complex are 0.2−0.3 Å shorter than for the Fe(II) and the Zn(II) complexes. This is in keeping with the fact that the d_{z^2} and $d_{x^2-y^2}$ orbitals are unoccupied in the low-spin d^6 Co(III) complex, but are singly and doubly occupied in the high-spin d^5 Fe(II) complex and the d^{10} Zn(II) complex. In three of the five isomers of the M(Bn-CDPy3)Cl complexes, the pyridyl donors are arranged meridionally (isomers A, B, and C) and two are facial (isomers D and E). Isomer C is calculated to be the most stable. If it was not for the cyclohexane ring, isomer A would be the mirror image of isomer C and is the next most stable isomer. For each of the metals considered, isomer B is ca. 8 kcal/mol less stable than C. In B, the two pyridyl rings are *trans* to each other and are nearly coplanar, whereas none of the pyridyl rings in isomers A and C lie in the same plane. The two facial isomers, D and E, are 10−16 kcal/mol less stable than C. Isomers D and E have the two pyridyl rings coplanar and *cis* to each other.

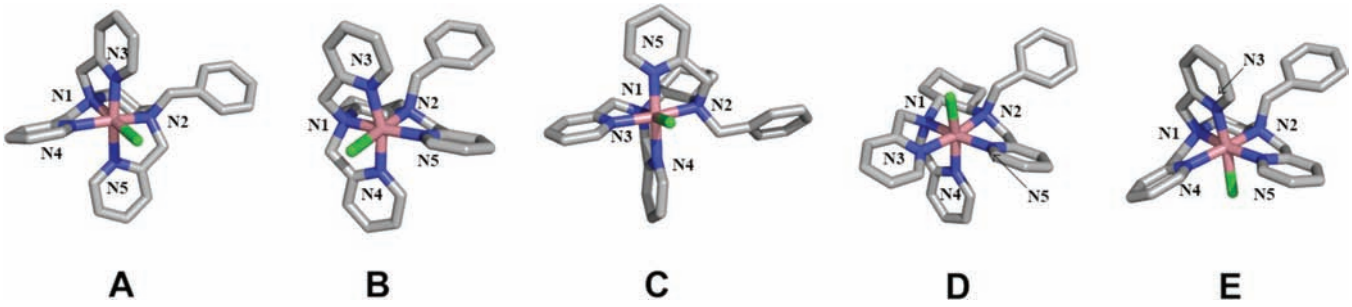

Figure 9. Isomers of M(Bn-CDPy3)Cl determined from calculations: A, B, and C display *mer* orientations of the pyridyl donors; D and E are *fac*.

Table 4. Relative Energies of the Five Isomers of $[Co(Bn\text{-}CDPy3)Cl]^{2+}$, $[Zn(Bn\text{-}CDPy3)Cl]^{+}$, and $[Fe(Bn\text{-}CDPy3)Cl]^{+}$ in kcal/mol

isomer	entire complex[a]	ligand only[b]	ligand−metal interaction[c]
C			
Co	0.00	0.00	0.00
Zn	0.00	0.00	0.00
Fe	0.00	0.00	0.00
A			
Co	7.12	2.65	4.47
Zn	2.49	0.86	1.63
Fe	2.79	0.96	1.83
B			
Co	7.79	3.79	4.00
Zn	7.76	3.25	4.51
Fe	8.34	3.26	5.08
D			
Co	15.73	5.70	10.04
Zn	12.44	2.73	9.71
Fe	13.12	3.29	9.83
E			
Co	13.45	3.15	10.31
Zn	12.44	2.73	9.71
Fe	12.41	2.79	9.62

[a] Energy of the M(Bn-CDPy3)Cl complex relative to isomer C. [b] Single-point energies of the complexes with the metal chloride removed, relative to isomer C; these energies reflect the differences in the ligand distortion energies in the various isomers relative to isomer C; the ligand distortion energies for isomer C are 20.64 and 1.08 kcal/mol greater for the Co and Fe complexes than for the Zn complex. [c] Entire complex energies minus the ligand-only energies; these energies reflect the differences in the electronic interaction between the ligands and the metal chlorides.

Both steric ligand distortion and ligand−metal binding energies contribute to the energy differences between the various isomers. The ligand distortion contributions are easily factored out by removing the metal chloride from the complex and computing the energy of the ligand frozen at the geometry of the complex. As shown in Table 4, the ligand of isomer C has the lowest distortion energy for each metal considered. Because of the shorter metal ligand bond distances, the ligand in the Co(III) complex C is 20 kcal/mol more strained than the ligand in the corresponding Fe and Zn complexes. For a given metal, the ligand of isomer A has the next lowest distortion energy, and those for the remaining isomers are 3−6 kcal/mol greater than for isomer C. The distortion energies of the ligands in the facial isomers D and E are not significantly higher than for the meridinal isomers A−C.

If the difference in the ligand distortion energy is subtracted from the relative energy of the isomers, one is left with differences in the electronic contribution arising from the metal−ligand interactions. As indicated in Table 4, the

Table 5. Comparison of X-ray Crystallographic Data and Calculated Structures for the $[Co(Bn\text{-}CDPy3)Cl]^{2+}$, $[Zn(Bn\text{-}CDPy3)Cl]^{+}$, and $[Fe(Bn\text{-}CDPy3)Cl]^{+}$ Cations[a]

	crystallographic data	isomer C	isomer A	isomer B	isomer D	isomer E
Co						
M−Cl	2.241(1)	2.244	2.243	2.254	2.248	2.279
M−N1	1.962(2)	1.989	1.999	1.971	1.976	1.987
M−N2	2.015(2)	2.044	2.049	2.056	2.053	2.036
M−N3	1.941(2)	1.966	1.989	1.961	1.983	1.973
M−N4	1.952(2)	1.971	1.957	1.983	1.996	2.010
M−N5	1.945(2)	1.970	2.007	1.954	1.949	1.988
Zn						
M−Cl		2.283	2.276	2.290	2.297	2.362
M−N1		2.331	2.341	2.217	2.216	2.247
M−N2		2.269	2.252	2.455	2.314	2.286
M−N3		2.175	2.228	2.227	2.242	2.268
M−N4		2.220	2.141	2.275	2.419	2.215
M−N5		2.242	2.361	2.109	2.125	2.165
Fe						
M−Cl	2.339(1)	2.269	2.267	2.270	2.282	2.340
M−N1	2.236(1)	2.307	2.319	2.245	2.246	2.257
M−N2	2.268(1)	2.308	2.298	2.435	2.311	2.304
M−N3	2.163(1)	2.144	2.213	2.218	2.260	2.240
M−N4	2.202(1)	2.184	2.124	2.233	2.316	2.213
M−N5	2.182(1)	2.222	2.284	2.104	2.145	2.187

[a] Bond lengths in Å and bond angles in deg; for atom numbering see Figure 9. For isomer C, the rmsd for the heavy atoms in the crystal structure versus calculated structure is 0.182 Å for $[Co(Bn\text{-}CDPy3)Cl]^{2+}$ and 0.139 Å for $[Fe(Bn\text{-}CDPy3)Cl]^{+}$.

electronic contribution for the *mer* isomers A−C is 5−10 kcal/mol more stabilizing than for the *fac* isomers, D and E. There is a delicate balance between the numerous factors in the electronic contribution, and it is not possible to single out one dominant term either by looking at the NBO analysis or by examining the geometric parameters. However, inspection of the structures provides evidence for the *trans* effect[63−65] and for interactions of the metal−ligand bonds with the π system of the pyridyl rings. For example, metal−pyridyl bonds *trans* to an amine nitrogen in isomers A−C are always shorter than the metal−pyridyl bonds *cis* to the amine (see Table 2). The Fe−N and Zn−N bonds *trans* to Cl are longer than the corresponding bonds *cis* to Cl (for low-spin d^6 Co(III), other factors contribute and the *trans* lengthening by Cl is not evident). Interactions of the pyridyl π orbitals with the metal−ligand antibonding orbitals are most clearly seen in the *fac* isomers. The M−N bonds aligned with the π orbital of the pyridyl *trans* to the Cl (e.g., *R*(Zn−N4) 2.215 Å and *R*(Zn−N2) 2.286 Å for Zn isomer E) are longer than the

(63) Burdett, J. K.; Albright, T. A. *Inorg. Chem.* **1979**, *18*, 2112–2120.
(64) Coe, B. J.; Glenwright, S. J. *Coord. Chem. Rev.* **2000**, *203*, 5–80.
(65) Anderson, K. M.; Orpen, A. G. *Chem. Commun.* **2001**, 2682–2683.

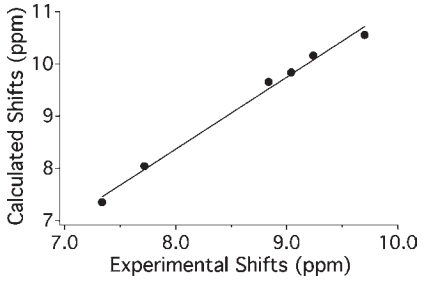

Figure 10. Comparison of calculated and observed chemical shifts of the three protons in the 2-position on the pyridyl rings in isomer C of $[Co(Bn\text{-}CDPy3)Cl]^{2+}$ and $[Zn(Bn\text{-}CDPy3)Cl]^{+}$ (R^2 = 0.992).

M−N bonds perpendicular to the π orbital (R(Zn−N5) 2.165 Å and R(Zn−N1) 2.247 Å, respectively).

Calculation of the excited states for isomer C of $[Co(Bn\text{-}CDPy3)Cl]^{2+}$ yields a weak transition at 532 nm comparable to the weak absorption observed at 550 nm. The longest wavelength transitions calculated for the other meridinal isomers are in the same region (541 and 535 nm for A and B, respectively); the transitions for the facial isomers were at shorter wavelengths (490 and 505 nm for D and E, respectively). Similar agreement is found for the iron complex: isomer C of $[Fe(Bn\text{-}CDPy3)Cl]^{2+}$ has a transition at 389 nm compared to the observed transition at 413 nm.

The ^{1}H NMR spectra for $[Co(Bn\text{-}CDPy3)Cl]^{2+}$ and $[Zn(Bn\text{-}CDPy3)Cl]^{+}$ were calculated for comparison with the experimental data. As shown in Figure 10, there is an excellent correlation between the calculated and observed chemical shifts for the three protons at the 2-position of the pyridine rings. For each complex, two of the resonances are downfield, while the third resonance is shifted upfield by approximately 1.5 ppm. The upfield shift is due to the shielding effect of the pyridyl ring situated directly below the 2-pyridyl proton, as shown in Figure 11. A similar effect is seen in calculations of the iron complex, but is complicated by a very large paramagnetic contribution. Other isomers of the cobalt, zinc, and iron complexes also show a large upfield shift for 2-pyridyl protons that are directly above the π system of a pyridyl ring (see Supporting Information).

Discussion

The experimental and theoretical data presented herein indicate that the chiral pentadentate ligand Bn-CDPy3 displays a significant thermodynamic preference for adopting the same coordination geometry in metal complexes of the general formula [M(Bn-CDPy3)Cl], regardless of the metal ion. This observation is noteworthy because five different coordination geometries are possible for the chiral ligand complexes of this formula. In the cases of the Co(III) and Fe(II) complexes, X-ray crystallographic data were used to determine the structure of the complexes. For the Zn(II) complex, 1D and 2D NMR data were consistent with the assigned structure. For the Fe(II), Co(III), and Zn(II) complexes, the calculations agreed well with the experimental data, including calculations that produced the same pattern of two downfield and one upfield resonance in the ^{1}H NMR spectrum for the 2-pyridyl C−H groups of the Co(III) and Zn(II) complexes.

In part, the origin of conformation control can be understood by contrasting the data for Bn-CDPy3 complexes with crystallographic data of the related complexes derived from the achiral ligand Bn-TPEN. Compounds of the general formula [Fe(II)(Bn-TPEN)X] all crystallize with the same conformation (Figure 12, X = Cl), having the X group *trans* to the basic amine donor N(1) and the three pyridyl donors N(3)−N(5) adopting the *mer* geometry. In addition, two pyridine N-donors, N(3) and N(4), adopt a coplanar conformation of their rings with respect to the Fe−X bond, while the third donor ring containing N(5) is perpendicular to that axis. Therefore, the fact that Bn-CDPy3 would prefer to adopt the same conformation upon coordination to a metal ion is not a surprise. On the basis of this analysis, three of the conformers shown in Figure 9 (B, D, and E) can be eliminated from consideration as the most stable because they do not possess an X group *trans* to the basic amine donor N(1). Only two complexes with Bn-CDPy3, conformers A and C, adopt this preferred geometry. In the case of the Bn-TPEN complexes, the energetic difference between A and C is not an issue, because these conformers are enantiomers; therefore they are isoenergetic. However, with the chiral ligand Bn-CDPy3, A and C become diastereomeric; therefore they can exist at different relative energies. It should be noted that the same conformational preference was assumed for the cation $[Fe^{IV}(O)(Bn\text{-}TPEN)]^{2+}$ based on paramagnetic ^{1}H NMR data, which indicated the same pattern of two downfield and one upfield shift for the 2-pyridyl C−H resonances[5] and on DFT calculations of conformational energies for different isomers.[5,66]

What is interesting in the case of Bn-CDPy3 is what distinguishes conformations A from C. Both have the same features: X group *trans* to N(1) and a *mer* geometry of three pyridyl N-donors, with two coplanar and one perpendicular to the M−X axis. Yet, conformation C is preferred over A by greater than 2 kcal/mol in the Zn(II), Fe(II), and Co(III) complexes. Our calculations have indicated that the origins of energetic control over geometry are born from the ligand in addition to the electronic preference (see ligand−metal interactions, Table 4). Inspection of the calculated structures indicates the ligand preference may be due to interactions between the cyclohexane ring and the groups surrounding the metal center. Namely, the calculations show 2.65 kcal/mol stabilization for the ligand in conformation C relative to A when the metal ion is removed from the Co(III) complex. Upon inspection of the metal complexes, there are no severe destabilizing interactions, such as eclipsing interactions, that are readily apparent in A and not in C that would explain why C is preferred. However, superimposing the structures shown in Figure 13 gives some insight into the origin of stereocontrol (additional figures can be found in the Supporting Information). In order to visualize the overlap between the two structures in the most effective manner, the enantiomer of structure A (*ent*-A) was generated to create the same stereochemistry around the metal center, while the stereochemistry of the diaminocyclohexane unit was inverted. The metal atom, the five nitrogens, and the chloride were superimposed to produce the overlapped structures. As shown in Figure 13, atoms surrounding the metal center exhibit good overlap, with the exception of the top pyridyl ring, which rotates slightly from structure C to *ent*-A. It is clear in C that the methylene hydrogen atom can occupy the cavity directly between two axial hydrogen atoms, as shown in Figure 13. In *ent*-A, because the cyclohexane ring has undergone a ring flip, an axial hydrogen atom occupies this

(66) Wang, Y.; Wang, Y.; Han, K. *J. Biol. Inorg. Chem.* **2009**, *14*, 533–545.

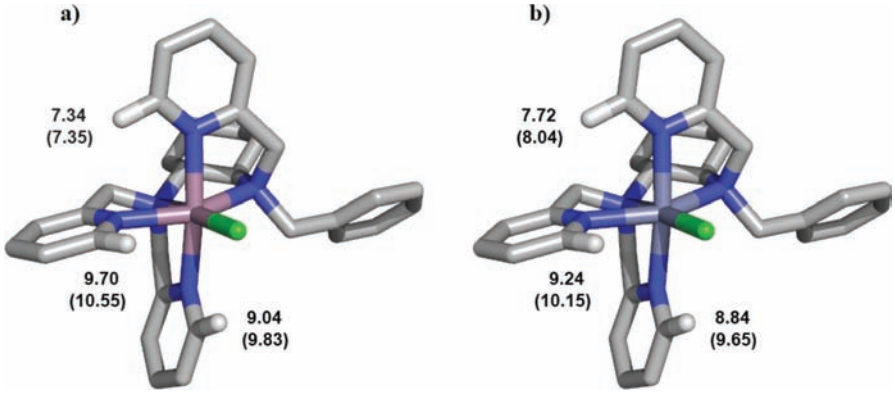

Figure 11. Observed and calculated (in parentheses) chemical shifts for the 2-pyridyl C−H protons (shown in white, other protons omitted for clarity) of (a) $[Co(Bn\text{-}CDPy3)Cl]^{2+}$ and (b) $[Zn(Bn\text{-}CDPy3)Cl]^{+}$.

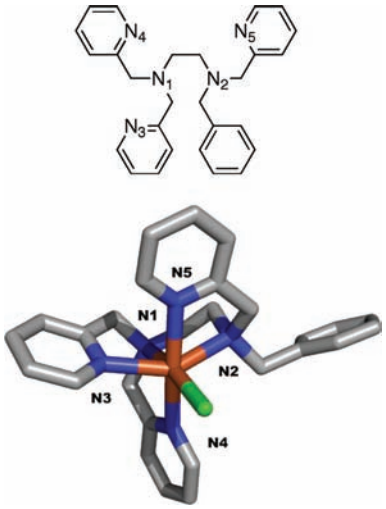

Figure 12. Structure of the ligand Bn-TPEN and model of the cation $[Fe(Bn\text{-}TPEN)Cl]^{+}$ generated using X-ray crystallographic data from ref [10]. The structure of the cation is similar to $[Fe(Bn\text{-}CDPy3)Cl]^{+}$, where the Cl group is in a *trans* conformation relative to N(1) and the three pyridyl N-donors N(3)−N(5) adopt a *mer* conformation, with two pyridine N-donors residing in a coplanar conformation with respect to the Fe−Cl bond, while the third ring is perpendicular to that axis.

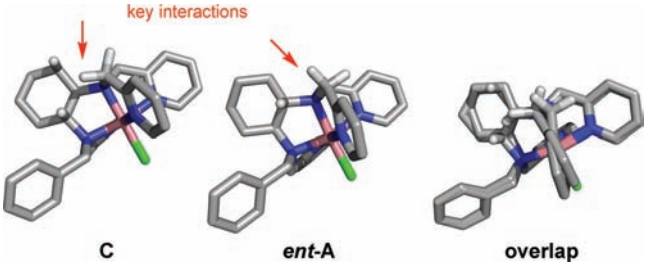

Figure 13. Calculated structures of the dication $[Co(Bn\text{-}CDPy3)Cl]^{2+}$ C, *ent*-A (see Figure 9), and an overlap of the two structures that illustrates the subtle differences between the two stereoisomers. All hydrogens except those creating key interactions are omitted for clarity. In the case of C, a methylene hydrogen can occupy a position directly above the cyclohexane ring and between two axial hydrogen atoms, whereas with *ent*-A, the pyridyl substituent rotates to avoid an unfavorable interaction with a closer axial hydrogen atom. See text for more details and Supporting Information for additional figures.

space; so in order to avoid an unfavorable nonbonding interaction, the 2-pyridyl methylene group rotates by 16° and bends by 18° relative to the Co−N−N−N plane in order to move away from the C−H group. This rotation also affects the bonding between the pyridine ring and the metal center, lengthening the distance by 0.018 Å. These interactions may explain both the ligand strain and ligand−metal binding contributions to the difference in energy between structures A and C in the Co(III) complexes. Similar interactions are found in the Zn(II) and Fe(II) complexes.

Conclusion

In conclusion we have described the synthesis of the chiral ligand (*R*,*R*)-Bn-CDPy3 and the characterization of zinc, iron, and cobalt complexes derived from the ligand. Structural data for these complexes revealed that a single coordination geometry is favored, by at least several kcal/mol, in metal complexes of Bn-CDPy3 out of five possible isomers. Theoretical data, which were in good agreement with experimental data, indicated that the preference for creating a single coordination geometry was due to both steric and electronic effects. Analysis of the calculated structures revealed some of the key interactions that enforced a strong stereoisomeric preference. Although the introduction of chirality into the pentadentate ligand certainly introduced more complexity in the coordination chemistry of the ligand relative to achiral ligands of this class, this work proves that control over geometry can be enforced and understood. A good understanding of these factors will pave the way for a selective synthesis of enantiopure complexes for applications in asymmetric catalysis.

Acknowledgment. J.J.K. would like to acknowledge Dr. Bashar Ksebati for help with NMR studies, Dr. Mary Jane Heeg for the X-ray crystallographic analysis, and Wayne State University for its generous support of this project. A.I.A. would like to thank the WSU IMR for support. J.A.S. would like to thank Marco Allard and Dr. Claudio Verani for their helpful discussions. H.B.S. and J. A.S. gratefully acknowledge support from grants CHE0910858 and GM058905-11, respectively.

Supporting Information Available: X-ray crystallographic tables, cif files for compounds **5**, **6**, and **8**, COSY, DEPT, HMQC, and NOESY NMR spectra for compound **9**, SCF energies calculated with TPSS and B3LYP functionals, Cartesian coordinates of compounds optimized with TPSS, full table comparing calculated structures and crystal structures, and calculated proton NMR chemical shifts for all structures. This material is available free of charge via the Internet at http://pubs.acs.org.